

The performance of the blue prime focus Large Binocular Camera at the Large Binocular Telescope

E. Giallongo¹, R. Ragazzoni², A. Grazian¹, A. Baruffolo², G. Beccari³, C. De Santis¹, E. Diolaiti³, A. Di Paola¹, J. Farinato², A. Fontana¹, S. Gallozzi¹, F. Gasparo⁴, G. Gentile², R. Green⁵, J. Hill⁵, O. Kuhn⁵, F. Pasian⁴, F. Pedichini¹, M. Radovich⁶, P. Salinari⁷, R. Smareglia⁴, R. Speziali¹, V. Testa¹, D. Thompson⁵, E. Vernet^{7,8}, and R. M. Wagner⁵

¹ INAF - Osservatorio Astronomico di Roma, Via Frascati 33, I-00040, Monteporzio, Italy

² INAF - Osservatorio Astronomico di Padova, vicolo dell'Osservatorio 5, I-35122 Padova, Italy

³ INAF - Osservatorio Astronomico di Bologna, Via Ranzani 1, I-40127 Bologna, Italy

⁴ INAF - Osservatorio Astronomico di Trieste, Via G. B. Tiepolo 11, I-34131 Trieste, Italy

⁵ Large Binocular Telescope Observatory, University of Arizona, 933 N. Cherry Ave., Tucson, AZ 85721-0065

⁶ INAF - Osservatorio Astronomico di Capodimonte, via Moiariello 16, I-80131, Napoli, Italy

⁷ INAF - Osservatorio Astronomico di Arcetri, Largo E. Fermi 5, I-50125, Firenze, Italy

⁸ European Southern Observatory, Karl-Schwarzschild-Str. 2, D-85748, Garching, Germany

Received ... ; accepted ...

ABSTRACT

Aims. We present the characteristics and some early scientific results of the first instrument at the Large Binocular Telescope (LBT), the Large Binocular Camera (LBC). Each LBT telescope unit will be equipped with similar prime focus cameras. The blue channel is optimized for imaging in the UV-B bands, the red channel is optimized for imaging in the VRIZ bands. The corrected field of view for each camera is about 30 arcmin of diameter and the chip area is equivalent to a 23×23 arcmin² field. In this paper we also present the commissioning results of the blue channel.

Methods. Several measurements have been obtained to assess the technical and scientific performance of the blue camera. Among others, astrometric distortion, flat fielding, ghosts and photometric calibration. These measurements have been used as input to a data reduction pipeline applied to the science data selected for the commissioning of the instrument.

Results. The measurements obtained during the commissioning showed that the technical performance of the Blue camera is within the expectation of the original project. Since the red camera is very similar to the blue one we expect similar performances from the commissioning that will be performed in the following months in binocular configuration. From a deep UV image obtained during the commissioning of the Blue camera we derived very deep UV galaxy counts in a large sky area down to $U(\text{Vega}) = 26.5$ showing that the Blue camera is the most powerful UV imager available at present and in the near future in terms of depth and large field of view. We have also emphasized the importance of LBC-Blue to increase the robustness of the UGR multicolour selection of Lyman break galaxies at redshift $z \sim 3$.

Key words. Instrumentation: detectors – Methods: data analysis – Techniques: image processing – Surveys – Galaxies: photometry

1. Introduction

The gain in information of an optical system depends both on its aperture and field of view (FoV). In this respect, imaging facilities in existing or planned telescopes have in most cases restricted capabilities: in most large telescopes, where the collecting area allows the detection of very faint sources, the FoV is often limited to about 7×7 arcmin² and the UV sensitivity is low. On the other hand wide field imagers at 4m (or smaller) telescopes are often optimized for relatively bright sources on larger FoV (i.e. MegaCam at CFHT, Boulade et al. 2003), but lack the sensitivity to reach deep magnitude limits (~ 28) especially in the UV band.

For these reasons an imager with a large FoV at an 8m class telescope is of fundamental importance to address the

presently still open problems in stellar and extragalactic astronomy.

The best example is the prime focus camera at the 8m Subaru telescope, Suprimecam (Miyazaki et al. 2002). This imager is fast and has a FoV of 34×27 arcmin². Noticeable examples of scientific use of this imager are represented by the search of very high redshift galaxies, the study of the formation and evolution of galaxies, the investigation of the structure of the Universe and the search for Kuiper Belt objects in the Solar system. However the optical correction needed to cover a wide wavelength interval can not cover simultaneously the UV band and the I band. For this reason, and also due to low sensitivity of the CCDs in the blue bands, Suprimecam is blind in the UV.

At the end of the 1990s, it became clear that the binocular configuration of the Large Binocular Telescope (LBT) (Hill et al. 2000) coupled with its mechanical design offered the unique opportunity to integrate a double prime focus

camera able to cover the widest wavelength interval from the UV down to the NIR H band.

The Large Binocular Camera (LBC, Ragazzoni et al. 2000, Pedichini et al. 2003, Ragazzoni et al. 2006) is a wide FoV instrument at the prime focus of the twin 8.4 meter Large Binocular Telescope (LBT). The LBT uses two 8.4-meter diameter honeycomb primary mirrors mounted side-by-side to produce a collecting area (110 square meters) equivalent to an 11.8-meter circular aperture. A unique feature of LBT is that the light from the two primary mirrors can be combined optically in the center of the telescope to produce phased array imaging of an extended field, requiring only minimal path length compensations, thus making interferometry easier than in completely independent telescopes.

The need for an instrument like LBC has been identified by several high-profile scientific programs that call for an increase in FoV and high-UV/IR sensitivity for deep imaging. In particular, these levels of performance are needed for programs that require a combination of a large FoV with extreme depth in a wide spectral interval that can only be provided by an imager at the prime focus of an 8m class telescope.

In Section 2 we provide a description of the two LBC cameras, while in Section 3 we detail the technical performance of LBC-Blue derived from the commissioning observations in 2006. In Section 4 we analyze in detail the case of an UV deep imaging survey in an extragalactic field and compare the results with those obtained from different instruments and telescopes. Conclusions are provided in Section 5.

2. The LBC camera

The Large Binocular Camera (LBC) is the unique wide-field double imager at the prime foci of the LBT.

The two channels are optimized for different wavelength ranges: the U, B, and V bands for the Blue channel (LBC-Blue), and the V, R, I, and Z bands for the Red channel (LBC-Red). Fig.1 shows the LBC-Blue instrument installed at the LBT, while Fig.2 describes the efficiency of the filter set available for LBC-Blue. The very fast final focal ratio (F/1.45) allows fast and deep imaging over a FoV of approximately 30 arcmin in diameter. Furthermore, since the two mirrors are mounted on the same pointing system, it will be possible to observe the same target simultaneously at different wavelengths, improving the operation efficiency. The fast prime focus configuration requires an optical corrector to compensate the aberrations introduced by the primary mirror. The unique binocular configuration of LBT allowed the optimization of the two correctors for different wavelength intervals. This makes slightly easier the design task since the achromaticity requirements on each channel are somewhat relaxed.

2.1. LBC Blue

The main difficulties in the design of a prime focus corrector for LBT are represented by the focal ratio of the primary mirror (F/1.14), the large telescope diameter (8.4m) and the parabolic shape of the mirror. The blue channel design can be described as a modification of Wynne's approach



Fig. 1. The LBC-Blue instrument installed at the prime focus of the first LBT telescope unit.

(Wynne 1996). The latter consists of three lenses able to mainly correct spherical aberration, coma and field curvature. In our design the second and third lenses are split into two elements and an additional lens is present with respect to Wynne's design: it is a positive meniscus with almost no net power, representing the window of the cryostat for the CCD. Due to the size of the primary mirror the largest lens of the corrector has a considerable diameter (810 mm) and weight (104 Kg). All the lenses are in fused silica, which ensures high throughput in the relevant wavelength range. The optical surfaces are spherical or plane, except lens #3, featuring an aspherical surface on the concave side; this surface is actually ellipsoidal and presents a departure from the best fit sphere of 0.7mm at the edge (Fig.3). Geometric distortion is not considered as an aberration, since it may be corrected by post-processing. Two filter wheels are placed between the last two lenses. The focal length of the optical corrector is 12180mm and the final focal ratio is F/1.45. The total throughput is 84%. The throughput considers the internal transmission of the SILICA lenses and the coating efficiency; it is an average figure for the U and B bands and does not consider the filter transmission.

The energy concentration of the instrumental PSF is very good: 80% of the energy is enclosed in a single CCD pixel (13.5 μ m in size or 0.2254 arcsec) both in the U and B bands which ensures good optical performance even in the best seeing conditions (FWHM \sim 0.4 arcsec). Although the Blue channel has been optimized for the U and B bands,

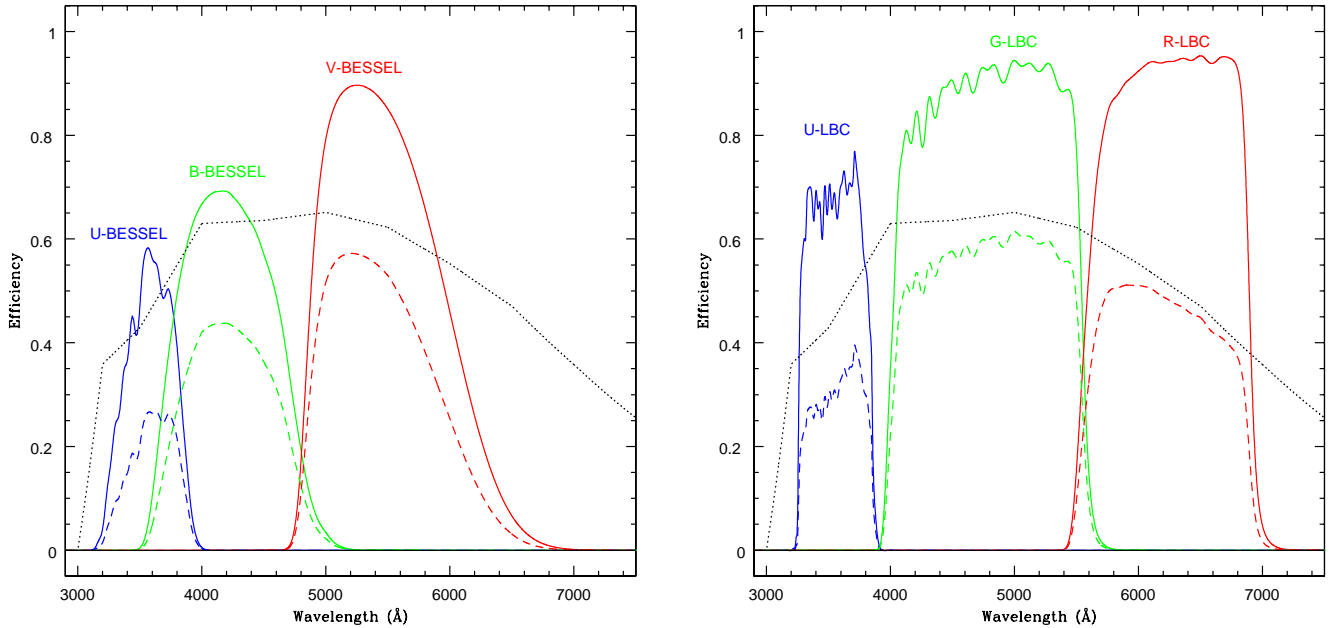


Fig. 2. LBC-Blue filter set. Bessel U, B, and V in the left panel, U-LBC, G-LBC, and R-LBC in the right panel. Dashed curves are the filter response curves derived after convolution with the overall LBC-Blue efficiency (the combination of CCD efficiency, mirror reflectivity, and optics transmission), which is shown as a dotted line.

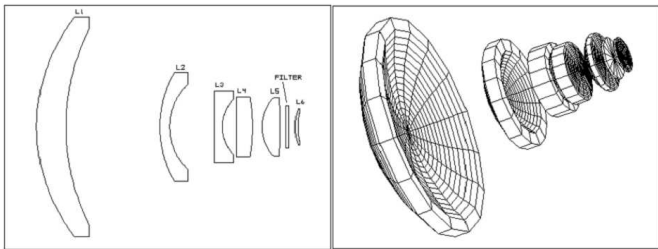


Fig. 3. LBC-Blue. 2D layer and 3D model of the optical corrector.

the performance is quite good also in the V and R bands, with 80% of the energy within 2×2 pixels. The geometric distortion, of pin-cushion type, is always below 1.75% even at the edge of the field (see Fig.4). The unvignetted FoV is 27 arcmin in diameter, as shown in Fig.5.

The mechanical design of the prime focus consists of two main parts: the hub that mounts the fixed lenses and the derotator which holds the filters wheels and the cryostat. Each one of the five fixed lenses is kinematically mounted into an INVAR frame, which is then connected to the steel hub through flexure elements to accommodate the differential thermal expansion of the two materials. For the same reason, the two main lenses, which are 810 mm and 400 mm in diameter, are mounted into their INVAR frames by means of special RTV pads, that are tailored to compensate for the differential thermal expansion of the glass and the INVAR.

The derotator decouples the imager from the corrector lenses and hosts two filter wheels, the shutter and the cryostat. Finally, the cryostat mount is suited to install all the instrument electronics on board the derotated structure. Concerning the servo controls of the instrument, each mo-

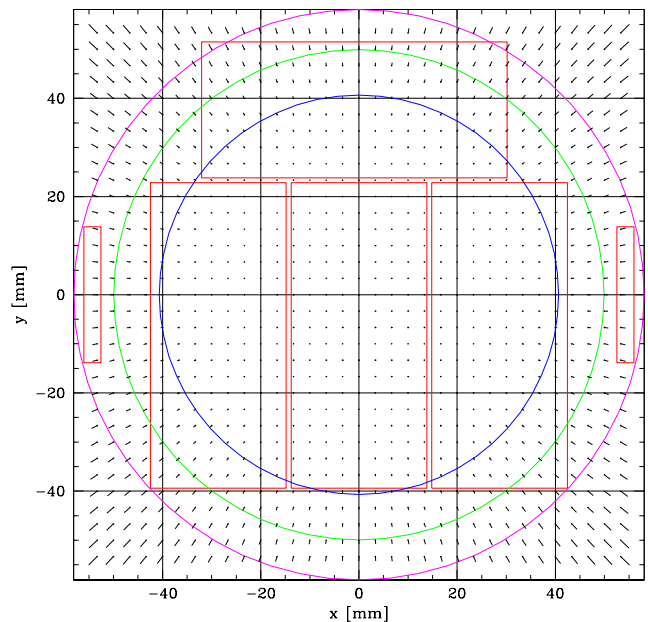


Fig. 4. The optical distortion map of LBC-Blue. The inner, middle, and outer circles mark the 1%, 1.5%, and 2% distortion limits, respectively. The geometric distribution of the four science chips and of the two technical arrays is also shown.

tor controller is addressed by the control PC as a network node by means of a TCP-IP protocol.

Each of the two cryostats was designed to cool down to 170K the detector flange that holds the scientific array of each camera composed of four E2V 42-90 chips and

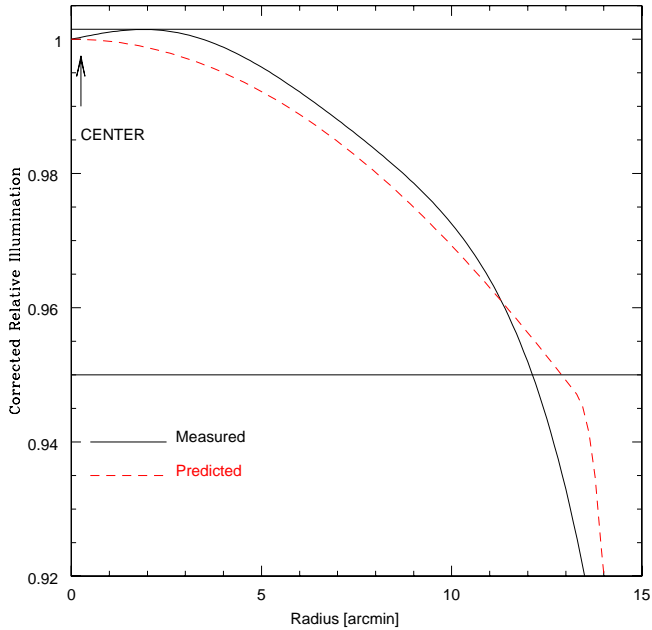


Fig. 5. Flat-field illumination profile in the R band corrected for pixel scale variation across the field. The expected profile from the optical design is also shown for comparison.

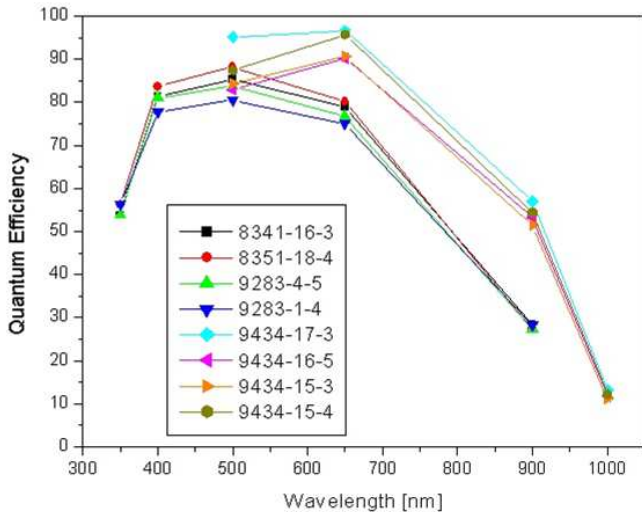


Fig. 6. Quantum efficiency of the science chips of the blue and red channel (higher points at 900 nm).

two more E2V detectors for technical use. The cryostat is composed of three independent modules: a stainless steel interface flange, a nitrogen vessel and a housing made of aluminium. This configuration allows to separate the electrical part (detector flange, cables, etc) from the cryogenic assembly, allowing an easy maintenance and upgrade of the two parts independently.

The peculiar component of this cryostat from the mechanical point of view is the bimetallic and monolithic vessel. It was designed with a spherical shape both to minimize the radiative thermal inlet and to make a quite compact instrument. With this geometry we obtain both a smooth cooling of the CCD baseplate and a good temperature sta-

bility, the latter being independent of the position of the camera. With a 10-liter fill of liquid nitrogen, the hold time of the cryostat is approximately 48 hours.

Two types of E2V detectors have been chosen to allow both the scientific data acquisition and the control of the instrument: an array of four E2V 42-90 (4608×2048 pixels) chips cover the corrected field with a sampling of about 0.2254 arcsec/pixel providing a scientific image of $23.6 \times 25.3 \text{ arcmin}^2$, while two E2V 42-10 of 256×2048 px are used to acquire short exposure images for guiding and wavefront control. The technical characteristics of the 42-90 are: $\text{QE} \gtrsim 80\%$ at the peak, charge transfer efficiency $> 99.999\%$, read-out-noise < 5 electrons at 1MHz, surface roughness $< 7\mu\text{m}$ peak to valley. The last requirement is imposed by the fast focal ratio (F/1.46) and is needed to keep the nominal optical quality of the image all over the focal plane. The gaps between the vertical chips are 1mm, which corresponds to 74 pixels or equivalently to 16.7 arcsec in the focal plane of LBC-Blue. The gap between the vertical chips and the horizontal one is instead 1.03mm (76 pixels, 17.2 arcsec).

There is a 5% loss of energy in the blue channel at the edge of the corrected field, while in the red channel this percentage of vignetting is well outside from the corrected area. The four science chips are placed in a rather unconventional fashion, with the fourth one rotated 90° with respect to the others, to optimally cover the corrected FoV (see Fig.4).

The CCD controller selected for the LBC camera was designed and produced by the Italian firm Skytech in collaboration with the LBC team. The core of the system is a programmable Xilinx FPGA used to accomplish several different tasks. The whole system is compact and uses only two half eurocard boards to be better hosted at the prime focus application of LBC. A good noise performance of $11e^-$ at 500 Kpix/s/ch is achieved despite the lack of a video preamplifier. In this configuration, the total readout time of the CCDs is 27 seconds.

The LBC shutter adopts a dual blade mechanics to ensure a uniform exposure on the overall field also at very low exposure times (0.1 sec). The accuracy ($\sim 2/1000$ sec) has been confirmed by laboratory tests using a laser trap.

Two filter wheels with five holes are available for each channel. At present U, B, and V Bessel filters as well as custom U, G, and R filters are available for the blue channel. Their spectral shapes convolved with the LBC efficiency are shown in Fig.2. The G filter of LBC is in practice equivalent to a standard Gunn-g filter, while the custom U and R filters are peculiar of the LBC-Blue instrument. The corresponding physical size of the filters is 155mm of diameter while the shutter used to cover the entire FoV of LBC-Blue is 470mm×186mm (Speziali et al. 2004).

The operation of the camera is handled by a graphical user interface and all the raw, calibration and telemetry data obtained so far are publicly available for the LBT partners in the LBC archive.

2.2. LBC Red

The red channel corrector is optimized for the wavelength range including the V, R, I, and Z bands, with a possible extension to the near infrared, up to $1.8 \mu\text{m}$ (J and H bands).

Even though the wavelength range of interest is approximately two times larger than for the blue channel, the red

design optimization has been somewhat easier, due to lower change of refractive index with wavelength toward the red part of the visible spectrum. Two glass choices have been initially investigated: silica and BK7. It should be stressed that neither silica nor BK7 ensure optimal transmission in the near infrared; on the other hand the main use of the instrument will be in the wavelength range from V to Z band and the extension to J and H should be intended as an additional facility. After a careful evaluation, BK7 has been chosen, due to the slightly better optical performance and the cheaper cost. The extension to the near infrared is based on the possibility to change the last lens (L6) while replacing the cryostat for the infrared detector.

The red channel design is very similar to the blue one, with 6 lenses (5 spherical and 1 aspherical) and a plane filter. The focal length, and hence the plate scale, are nominally equal to the blue channel design. Also the geometric distortion has been forced to the same value, in order to make the data reduction process more straightforward. The energy concentration at the wavelengths of interest is always well within the goal of 80% of the energy within a single CCD pixel. The total throughput is 82%.

The mechanical design of the red channel is very similar to the Blue channel case, considering the size of the lenses, their distances and especially the focal plane region and filter wheels. The major difference is represented by the different thermal behaviour of BK7 compared to SILICA.

The red channel is equipped with 4 high resistivity deep depletion 42-90 E2V detectors which are optimized for high efficiency at longer wavelengths. The QEs of the four chips are shown in Fig.6 and the technical characteristics are similar to the chips selected for the blue channel.

The red camera will be commissioned at the end of 2007 and the binocular configuration will be available at the beginning of 2008. More details on the instrument are available on the LBC web site at <http://lbc.oa-roma.inaf.it/>.

3. The commissioning run of LBC-Blue

The LBC-Blue camera was the first instrument installed at the LBT and for this reason was also used for the commissioning of the first LBT telescope.

During the commissioning phase performed in the period October-December 2006, a lot of astrometric and photometric fields were observed in order to characterize the instrument. A detailed description is given in the next section. Some nights were also dedicated to scientific targets in order to test the performance of the instrument.

The targets were chosen to encompass a variety of open issues that LBC could address in the near future. Some examples include the nearby galaxy cluster CL2244-02 which acts on a distant galaxy producing a spectacular gravitational arc observed by LBC during a night with 0.45 arcsec seeing in the U band (see Fig.7). This image shows that it is possible to use LBC to study strong gravitational lensing if an efficient service observing is carried out to select the best seeing conditions. Several star clusters were observed, NGC7789, NGC2419, and M67, to analyze the technical performance related e.g. to the variation of the PSF profile across the overall LBC FoV and to the analysis of the astrometric distortions due to the complex optical correctors described in Section 2. Extragalactic targets, like the galaxy cluster Abell576, the Subaru XMM Deep Survey (SXDS) and the quasar Q0933+28 field were observed to

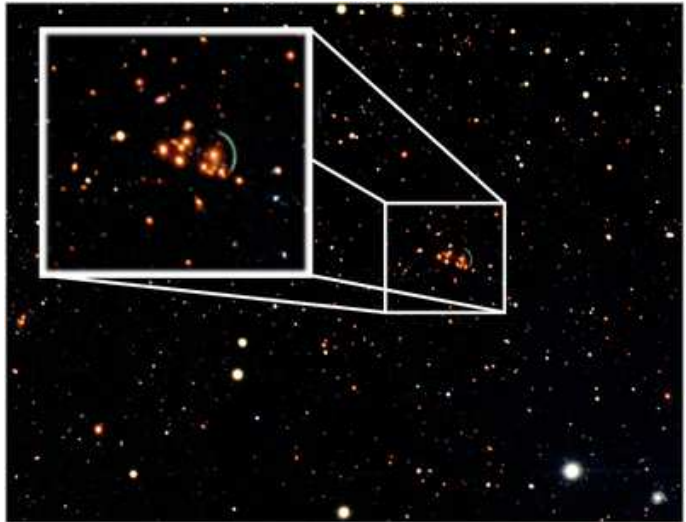


Fig. 7. The galaxy cluster CL2244-02 and its gravitational arc as seen in the central chip of LBC-Blue (only $\sim 10\%$ of the entire FoV is shown here). The FWHM is particularly good, 0.45 arcsec in the U band and 0.55 in the B and V bands.

Table 1. Read-out noise and gain factors for the four chips of LBC-Blue.

Parameter	Chip #1	Chip #2	Chip #3	Chip #4
R.O.N. e^-	11.4	11.6	11.6	11.2
e^-/ADU	1.96	2.09	2.06	1.98

derive the magnitude limits in deep imaging surveys and to add deep UV-B images to the multicolour information already available in these fields for the analysis of the evolutionary properties of the faint distant galaxies.

3.1. Technical performance of LBC-Blue

The presence of a pre-scan and an over-scan in each image allows a correct subtraction of the bias which is stable in time. Dark current is also negligible considering that exposure times of a single image are usually smaller than 15 minutes. The read-out noise and e^-/ADU conversion factor (gain) have been measured using the “variance method” on flat field sequences and were found to be conformal to the laboratory measurements. Chip to chip small differences were found and are summarized in Table 1.

The camera provides a linearity residual error smaller than 1% over the whole 16 bit dynamic range ($120000 e^-$). The detector full well limit before blooming is greater than $150000 e^-$.

In most imagers based on CCD mosaics, electronics ghosts due to the video channel’s cross-talk are often present and are removed using software procedures specifically designed to this aim (see for example <http://lbc.oa-roma.inaf.it/commissioning/xtalk.html>) especially when bright saturated sources are present in the field of view. For LBC the cross talk coefficients are always of the order of 3×10^{-5} .

Flat fielding can be derived from twilight sky and night sky data. Fig.5 shows the radial profile of the flat-field illumination as of April 2007. The dome-shaped profile is the result of intrinsic illumination pattern, with residual

scattered light affecting the central region of the FoV and vignetting affecting the outer regions of the FoV. All the curves are normalized to unity in the center. In the figure the profile originating from the sky ghost is visible at 0.15% level nearby the geometrical center (pixel $x=1024$ $y=2919$ of chip no. 2). The radial profile predicted by the original design is shown for comparison. Any difference is smaller than 1% up to about 13 arcmin off axis.

Being a prime focus camera, distortions are expected to be quite relevant. The original design predicted a corrected field extending out to about 10 arcmin from the center. Nevertheless, optical distortions produce essentially two effects: variation of the pixel scale in the FoV and deformation of the PSF. The first effect has been computed from simulations and tested with images of moderately crowded fields. It is corrected through an astrometric solution process estimated from the images. The second effect is partially recovered by resampling the images and using a variable PSF model or using sufficiently large photometric apertures. Both techniques were used to measure the flux of standard stars, and the results were found to be fully consistent.

The main optical distortion map is reproduced in Fig.4. The estimate of the astrometric solution is done through a three-steps process using the software package *AstromC* developed by M. Radovich: this package is a porting to C++ of the Astrometry software described e.g. in Radovich et al. 2004. The final astrometric solution is similar to the theoretical pre-solution derived from the original optical design. Second-order corrections vary from frame to frame because of different elevation, filter or position angle. These variations are however very small. Filter to filter variation is of the order of 0.01%, corresponding to about 1 pixel at the edge of the FoV. The pixel scale at the center is $0.2275'' \pm 0.0001$ and the median value is $0.2254'' \pm 0.0001$ with filter-to-filter variation affecting the fourth decimal digit. The corrected individual frames can be resampled to a constant pixel scale and stacked to a final image mosaic.

In Fig.8 we show an example of the mosaic LBC-Blue field of view in the U-bessel filter after applying various steps of the reduction procedure. The raw image in Fig.8 (a) shows both the effects due to vignetting and sky concentration caused by the geometrical distortion. In Fig.8 (b) the same mosaic image is shown after cross-talk correction, bias subtraction and flat-fielding which removes the vignetting effect. In Fig.8 (c) the science mosaic is shown after removal of the geometrical distortion by re-sampling to a constant pixel scale. The quality of the PSF over the entire FoV of LBC-Blue does not depend on the radial distance from the optical center. This is also true for the ellipticity of stars in the field, which is always below 0.05, with a median value of 0.02. Thus, the uncertainties in telescope guiding and the optical distortion do not affect significantly the quality of the image at large distances from the center.

We have also analyzed images taken during the commissioning and science demonstration time (SDT) to quantitatively estimate the presence and magnitude of ghosts due to bright stars. The Bessel U, B, V, and custom G and R filters do not show measurable ghosts, in agreement with our expectations. Indeed, according to simulations, the ghost due to a bright star falls at the center of the bright star itself and it is 12 magnitude fainter. In the interference U-LBC filter the primary ghosts due to bright stars are more evident. The primary ghost of a UV bright star has the

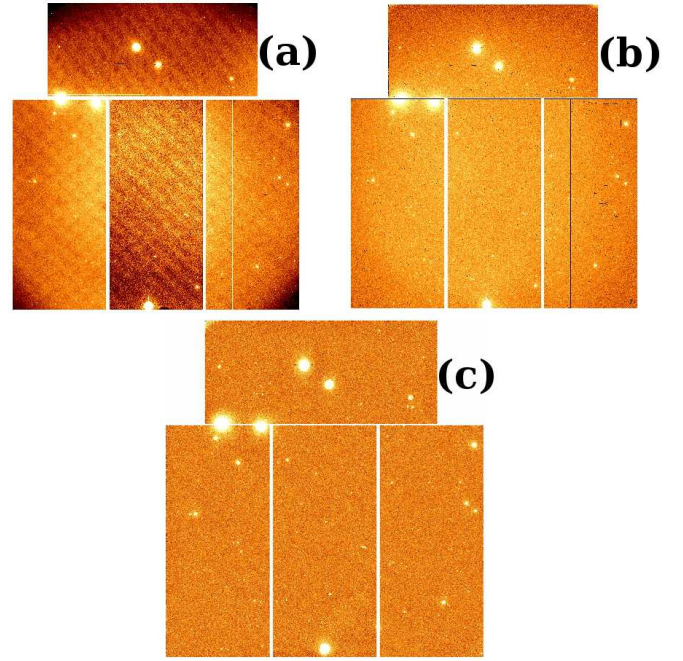


Fig. 8. (a) Raw LBC-Blue image. (b) The same image after flat-fielding correction. (c) The same image after resampling to a constant pixel scale.

shape of a diffuse circle. To estimate the amount of flux in the primary ghost we first built a model for the PSF from stars with peak intensity less than 20000 ADU and then used this model PSF to fit the non saturated wings of bright stars. After PSF subtraction, two components remain: an intense circular ring centered on the bright star (diameter=75 pixels) and a diffuse large component (diameter=200 pixels) of smaller intensity, shifted respect to the bright star in radial direction. We have computed the total intensity of the inner bright component and of the diffuse, larger one finding a value of 2.8 ± 0.7 per cent. We do not find evidence of dependence of the ghost intensity on the distance from the center field. The ghost intensity is independent of the position angle of the camera or elevation of the telescope. No secondary ghosts are measurable on the science data.

Calibration equations have been obtained for two photometric nights during the commissioning run of November 2006 in the Bessel U, B, and V filters. The equations adopted were of the kind:

$$V = v + z.p. + c.t. \times (b - v) + k_V \times X_V \quad (1)$$

where $z.p.$ is the photometric zero point, $c.t.$ is the colour term, k_i is the atmospheric extinction coefficient in the i -th band and X_i , the airmass in the same band. We calibrated V and B versus the colour $b - v$, while filter U has been calibrated versus $u - b$. Photometric standards have been obtained from the Landolt et al. 1992 catalog, namely from the fields SA98 and SA113. These fields also contain a large number of additional standards measured by P.B. Stetson and available from the CADC web site. A supplementary catalog from Galadi-enriquez et al. 2000 has been used as well to increase the sample of U standards (Stetson standards have only B, V, R, and I band magnitudes) and to have a standard field close to the zenith for a better

Table 3. Observations of the Q0933+28 field with LBC-Blue

Filter	maglim(10σ) Vega mag	maglim(1σ) Vega mag	seeing arcsec	texp hours
U-BESSEL	25.13	27.73	1.06	3.00
G-LBC	26.01	28.51	0.83	0.45
R-LBC	24.97	27.47	1.22	0.50

The magnitude limits are computed in a circular aperture two times the FWHM in each band.

fit of the atmospheric extinction. The fits obtained are remarkably good and their internal errors very small. The photometric accuracy in the overall field is of the order of 0.01 mags. The values for the coefficients, with the relative uncertainties are reported in Table 2. For the G and R filters only zero points have been obtained so far using SDSS secondary standard fields, while the U-LBC filter was not available during the commissioning phase in 2006.

3.2. A test for deep imaging in the UV: the Q0933+28 field

To test the capabilities of LBC-Blue in the field of deep extragalactic surveys over large areas of the sky, we observed a field centered around the bright QSO Q0933+28 at $z=3.42$ (Veron-Cetty & Veron 2006). This field has been observed by Steidel et al. 2003 in the UGR filter set and was the target of an intensive spectroscopic campaign by Steidel and collaborators, which resulted in a hundred of galaxy spectra down to $R = 25.5$ AB mag in the redshift interval $1 \leq z \leq 4$ in this field. It is thus ideally suited to test LBC-Blue performance in the field of extragalactic astronomy. In particular a deep U-BESSEL image has been obtained in this field. The details of the observations are given in Tab. 3.

Raw LBC images were reduced with the LBC Pipeline, a collection of C and Python scripts optimized for LBC data analysis. The software performs cross-talk correction, bias subtraction (line by line, fitting the pre-scan and the over-scan), flat-field normalization. Then, we applied the astrometric solution given by AstromC to the provided frames and stacked them into a single mosaic using the Swarp package¹. The astrometric procedure uses positions and fluxes from overlapping sources in different exposures to simultaneously optimize the internal astrometric accuracy and derive a relative photometric calibration of the stacking. Then absolute calibrations were obtained using photometric standard fields (Landolt and/or Stetson) observed in the same night. We used the photometry in the Stone fields (Stone 1997) to calibrate the G and R filters and obtain a zero point for them. Part of the LBC field during commissioning was affected by scattered light, for this reason the total area of the Q0933+28 field was limited to 478.2 arcmin².

3.3. Deep U band galaxy counts

In order to test the efficiency of the LBC-Blue for deep photometry in the UV band over a large FoV we have computed the number counts of galaxies in the U band, where 3 hours of observations with average seeing conditions ($FWHM \sim 1$ arcsec) were obtained in the Q0933+28

field. We have used SExtractor (Bertin & Arnouts 1996) to derive the photometric catalog. For objects with area greater than that corresponding to a circular aperture of radius equal to the FWHM, we used the isophotal magnitudes provided by SExtractor. For smaller sources we computed magnitudes in circular apertures with diameter equal to 2 times the FWHM. This allows us to avoid the well known underestimate of the flux of faint galaxies provided by the isophotal method. To isolate the few stars from the numerous faint galaxies in this field, we relied on the class_star classifier provided by SExtractor.

Raw counts are shown in Fig.9 where a clear decrease is apparent for $U(Vega) > 26.4$. Thus an estimate of the completeness level should be performed in order to evaluate the amount of correction to the raw counts at the faint limits. This has been evaluated including in the real image 1000 simulated galaxies per magnitude bin in the magnitude interval $U(Vega) = 24 - 27$ using the standard "artdata" package in IRAF. For simplicity disk galaxies are included with convolved sizes typical of real galaxies in the magnitude interval $U(Vega) = 24 - 25$, i.e. with $FWHM \sim 2.5$ arcsec. The resulting 50% completeness level is measured at $U(Vega) = 26.5$. The corrected counts are shown in the same Fig.9. Given the wide magnitude interval from $U(Vega) = 19$ to $U(Vega) = 26.5$ available in the present survey, the shape of the counts can be derived from a single survey in self-consistent way, possibly avoiding offsets due to systematics in the photometric analysis. A clear bending is apparent at $U(Vega) > 23.5$. To quantify the effect we fitted the shape of the counts in the above magnitude interval with a double power-law. The slope changes from 0.62 ± 0.1 to 0.22 ± 0.04 for magnitudes fainter than $U_{break} = 23.2$. The uncertainty in the break magnitude is however large, ~ 0.8 .

In Fig.9 we compare our number counts with those derived by shallow surveys of similar area (GOYA by Eliche-Moral et al. 2006; Hawaii HDFN by Capak et al. 2004; VVDS-F2 by Radovich et al. 2004), and with deeper pencil beam surveys (WHT, HDFN, and HDFN by Metcalfe et al. 2001). In particular, the WHT galaxy counts (Metcalfe et al. 2001) are based on a 34h exposure time image reaching $U(Vega) = 26.8$ but at the much lower 3σ level in the photometric noise and in an area of ~ 50 arcmin², while the GOYA survey at the INT telescope is complete at 50% level at $U(Vega) = 24.8$. These counts are shown together with the two pencil beam surveys in the Hubble Deep Fields (Metcalfe et al. 2001).

The agreement with the GOYA survey (900 sq. arcmin.) is remarkable, and suggests that once big areas of the sky are investigated, the effects of cosmic variance are slightly reduced. Deep pencil beam surveys (HDFN, HDFN) can go about 1 magnitude deeper than our present magnitude limit but required much longer exposure times. The present UV counts obtained during the commissioning of LBC-Blue are the deepest obtained so far from ground-based observations in large sky area that are not affected by cosmic variance. Deeper observations are expected with LBC-Blue in fields with larger exposure times and with more efficient UV filters.

It is interesting at this point to compare the LBC-Blue performance in particular with that of MegaCam at CFHT, since Suprimecam at Subaru is not efficient in the UV. LBC is of course 4 -4.5 times faster than MegaCam at CFHT in the UV-B bands but the field of view is about 1/6 deg².

¹ <http://terapix.iap.fr/>

Table 2. Photometric calibration coefficients

Filter	Zero Point	Colour Term	Extinction	corrAB
U-BESSEL	25.36 ± 0.03	0.036 ± 0.009 (u-b)	-0.48 ± 0.02	0.87
B-BESSEL	28.00 ± 0.02	-0.123 ± 0.003 (b-v)	-0.22 ± 0.01	-0.07
V-BESSEL	28.12 ± 0.01	0.021 ± 0.005 (b-v)	-0.15 ± 0.02	0.01
G-LBC	28.59 ± 0.02			-0.11
R-LBC	27.63 ± 0.02			0.13

The zero points are in the Vega photometric system, and the AB magnitude can be derived using the relation $mag(AB) = mag(Vega) + corrAB$. The U, B, and V filters are the Bessel ones, while G and R filters are peculiar of LBC-Blue. Only zero points are available for the G and R filters. The U-LBC filter was not available during the commissioning phase in 2006.

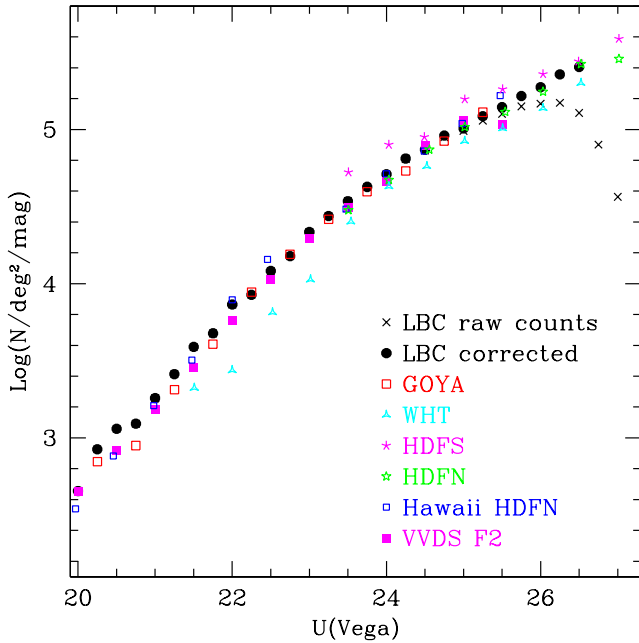


Fig. 9. Number counts of galaxies in the U-BESSEL band for the Q0933+28 LBC field. Magnitudes are in the Vega system. We compare our counts with shallow surveys of similar area (GOYA, Hawaii HDFN, VVDS F2), and with deeper pencil beam surveys (WHT, HDFN, HDF5).

Thus LBC is optimized for very deep images on relatively smaller areas. We note however that the high LBC UV efficiency allows the use of UV filters centered at shorter wavelengths (355 nm) respect to the MegaCam one (375 nm) providing UV magnitudes very similar to the standard Bessel system. Moreover, considering its final binocular configuration the LBC camera will double its global efficiency in multicolour imaging.

3.4. UV dropout galaxies at high redshifts

The field we have selected for the commissioning test of the blue channel is one of Steidel’s fields used for the search of Lyman break galaxies at $z \sim 3$. For this field original U, G, and R images, a multicolour UGR catalog and spectroscopic information are made publicly available by Steidel and collaborators and are used for comparison with the LBC images.

It is well known that an efficient method to select unobscured or modestly obscured star forming galaxies at high

redshifts is the Lyman break technique, that is effective in detecting high redshift Lyman break galaxies (LBGs) at $2.8 \leq z \leq 3.7$. This selection, adopted by Steidel and collaborators (e.g. Steidel et al. 1999; Adelberger et al. 2004) is based on the UGR filter set and exploits the strong absorption present in the UV band of these galaxies (UV dropout) caused by the redshifted Lyman continuum absorption produced by the interstellar neutral hydrogen of the same galaxies. Extensive spectroscopic follow up showed this multicolour selection to be highly effective (see e.g. Adelberger et al. 2004).

We have applied the same method with our UGR filter set of the blue channel to test by means of a deep U band image the advantage of an efficient UV imager at an 8m class telescope.

We have used the R image of the Q0933+28 field to obtain a catalog of galaxies whose magnitude limits at different σ levels are reported in Tab.3. We have used SExtractor (Bertin & Arnouts 1996) in dual-image mode to derive the photometry in the other filters for sources detected in the R band, which was used as the detection image. We smoothed with a gaussian kernel each band to reproduce the FWHM of the worst image obtained in the R band. In this way the stellar FWHM of the images are the same and the colours can be computed in the same object area.

The U-BESSEL and G filters of LBC-Blue are similar to the U and G filters used by Steidel and collaborators, while the R-LBC filter is very different from their R, since it is peaked at relatively shorter wavelengths because of the throughput decline of LBC-Blue beyond $\lambda = 7000 \text{ \AA}$ (see Fig.2). Comparing our multiband photometry with the publicly available catalog of the Q0933+28 field by Steidel et al. 2003 and on the basis of synthetic colours predictions by galaxy spectral synthesis models, we derived the colour equation to translate Steidel’s colours into the LBC photometric system, which resulted in $(G - R)_{LBC} = 0.7(G - R)_{Steidel} + 0.05$.

We have modified the colour selection criteria of Adelberger et al. 2004 taking into account the difference in the G-R colour and obtaining the following colour selections: $-0.25 \leq G - R \leq 0.9$ and $U - G \geq (G - R) + 1.0$ for Lyman break galaxies in the redshift interval $2.8 < z < 3.5$.

In Fig.10 (left panel) we plot the U-G versus G-R colour for all the galaxies in the Q0933+28 field using the original photometry by Steidel and highlight the selection criteria for LBGs galaxies. We also show the spectroscopically confirmed LBG galaxies by Steidel’s team, with 10 out of 24 galaxies resulted at lower redshifts ($z < 2.8$) although being in the colour region expected for LBGs. Only two out of these ten galaxies are found at redshift ≤ 2.2 .

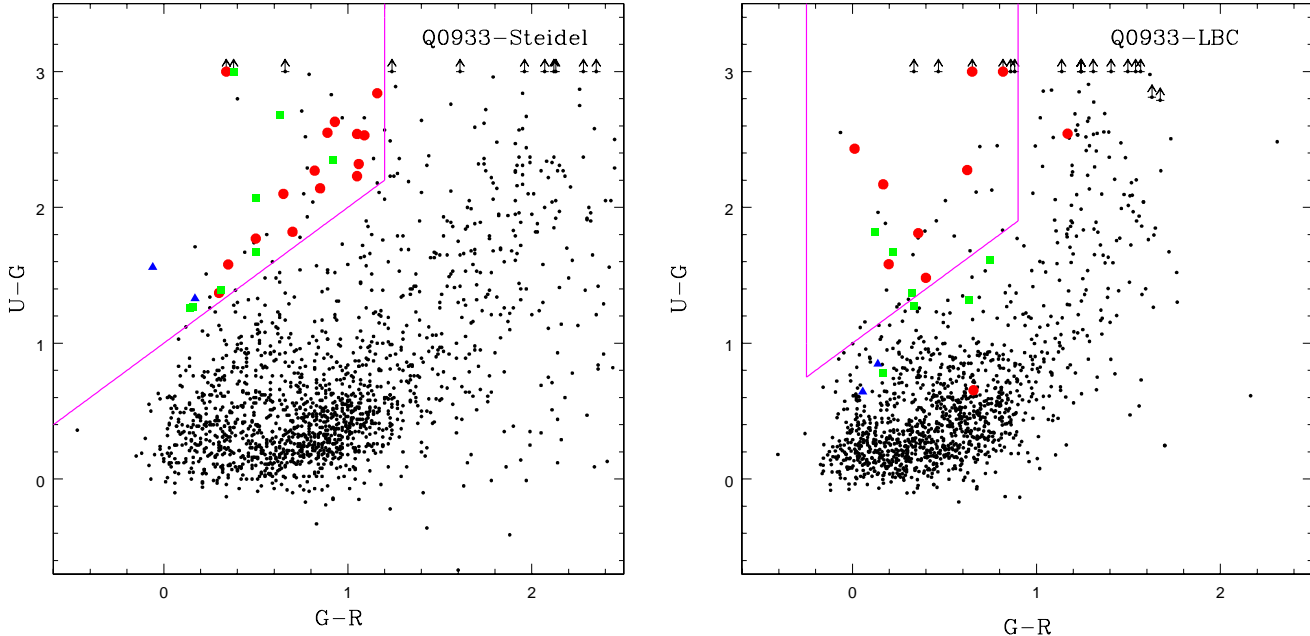


Fig. 10. Left panel: selection of LBGs in the field by Steidel in the $U-G$, $G-R$ colour diagram. Circles, squares, triangles are star-forming galaxies at $R \leq 24.5$ spectroscopically confirmed at $2.8 < z < 3.7$, $2.2 < z < 2.8$, and $1.4 < z < 2.2$, respectively. Right panel: same as in the left panel but using the colour catalog from the LBC images. Note that some galaxies at $z < 2.8$ are now correctly out of the LBGs region.

In Fig.10 (right panel) we show the same plot derived from the U, G, and R LBC images. In this comparison we restrict the analysis to the original Steidel’s area of $\sim 9 \times 9$ arcmin². We show with triangles, squares, and circles the galaxies in the redshift ranges analyzed by Steidel and collaborators: $1.4 < z < 2.2$, $2.2 < z < 2.8$ and $2.8 < z < 3.5$, respectively. In this case most of the LBGs candidates confirmed to be at lower spectroscopic redshifts are in general bluer, i.e. brighter in UV and in most cases lie consistently outside (or nearby, given the photometric noise) the LBGs colour region. Thus, even limiting the galaxy catalog to relatively bright objects with $R < 24.5$ the robustness of the UV dropout colour selection technique of LBG galaxies at $z \sim 3$ increases when very deep UV images as obtained by LBC are used.

An attempt in this direction was recently performed by Sawicki & Thompson 2005 who used very deep UGRI images obtained at Keck to produce a fainter sample of Lyman break galaxies at redshifts $z = 2, 3, 4$. However the greater UV sensitivity and larger field of view of LBC makes this instrument ideal to look for high redshift galaxies especially in the context of the study of the large scale structures at high redshift.

4. Conclusions

In this paper we have described the first instrument at the LBT telescope, the prime focus large binocular camera (LBC). The instrument has a binocular configuration with two channels, the blue channel with a good overall efficiency in the UV band and the red channel with good efficiency in the V-z bands.

We have also shown the technical characteristics of the blue channel derived from the commissioning data of LBC-Blue.

- The corrected optical field is ~ 30 arcmin of diameter with $< 5\%$ loss of energy within ~ 25 arcmin. The total throughput of the optical corrector is 84%.
- The optical distortion is always $< 1.75\%$ even at the edge of the field and it is removed with a specific SW package.
- The optical quality ensures an energy concentration of 80% within a pixel of $\simeq 0.2254$ arcsec in the overall corrected field. The active control of the optical quality can provide images as sharp as FWHM=0.5 arcsec even in the UV band.
- Ghost images produced by the whole optical system are always negligible when glass filters are used (Bessel U,B,V). The total intensity of the primary brightest ghost is $\sim 2.8\%$ when the wide interference UV filter is used. The primary ghost is centered on the original source position. Ghost images produced by the electronics cross-talk are as small as 3×10^{-5} and can be easily removed during data reduction.

We have also described some scientific observations planned for the commissioning to assess the performance of LBC-Blue.

- We have obtained very deep UV galaxy counts in a deep pointing with a total exposure time of 3h reaching $U(Vega)=26.5$, after correction for incompleteness. The wide magnitude interval ($U(Vega) = 19 - 26.5$) in our galaxy counts allowed a direct evaluation of the shape of the UV counts which shows a bending at about $U(Vega) = 23.2$ with a change in slope from 0.62 to 0.22 at the faint end.

- The same LBC area includes a quasar field where extensive study of Lyman break galaxies at redshift $z \sim 3$ is available. We have reproduced with our UGR filter set the well known multicolour selection of LBGs showing that the robustness of the UV dropout method for the selection of star-forming galaxies at $z \sim 3$ increases when very deep UV images can be used as obtained by LBC at an 8m class telescope like LBT.

Acknowledgements. Observations have been carried out using the Large Binocular Telescope at Mt. Graham, Arizona, under the Commissioning of the Large Binocular Blue Camera. The LBT is an international collaboration among institutions in the United States, Italy and Germany. LBT Corporation partners are: The University of Arizona on behalf of the Arizona university system; Istituto Nazionale di Astrofisica, Italy; LBT Beteiligungsgesellschaft, Germany, representing the Max-Planck Society, the Astrophysical Institute Potsdam, and Heidelberg University; The Ohio State University, and The Research Corporation, on behalf of The University of Notre Dame, University of Minnesota and University of Virginia. We thank C.C. Steidel and collaborators for the public availability of their images and spectroscopic redshifts of the Q0933+28 field. We thank the anonymous referee for useful comments which improve the clarity of the paper.

References

- Adelberger, K. L., Steidel, C. C., Shapley, A. E., et al. 2004, ApJ, 607, 226
- Bertin, E. & Arnouts, S. 1996, A&AS, 117, 393
- Boulade, O., Charlot, X., Abbon, P., et al. 2003, SPIE, 4841, 72
- Capak, P., Cowie, L. L., Hu, E. M., et al. 2004, AJ, 127, 180
- Eliche-Moral, M. C., Balcells, M., Prieto, M., et al. 2006, ApJ, 639, 644
- Galadi-enriquez, D., Trullols, E., Jordi, C. 2000, A&AS, 146, 169
- Hill, J. M., et al. 2000, in Science with the Large Binocular Telescope, ed. T. Herbst (Heidelberg:Neumann Druck)
- Landolt, A. U. 1992, AJ, 104, 372
- Metcalfe, N., Shanks, T., Campos, A., McCracken, H. J. & Fong, R. 2001, MNRAS, 323, 795
- Miyazaki, S., et al. 2002, PASJ, 54, 833
- Pedichini, F., et al. 2003, Proc. SPIE, 4841, 815
- Radovich, M., Arnaboldi, M., Ripepi, V. et al., 2004, A&A, 417, 51
- Ragazzoni, R., et al. 2000, Proc. SPIE, 4008, 439
- Ragazzoni, R., et al. 2006, Proc. SPIE, 6267, 33
- Sawicki & Thompson 2005, ApJ, 635, 100
- Speziali, R., Pedichini, F., Di Paola, A., et al. 2004, SPIE, 5492, 900
- Steidel, C. C., Adelberger, K. L., Giavalisco, M., Dickinson, M., Pettini, M., 1999, ApJ, 519, 1
- Steidel, C. C., Adelberger, K. L., Shapley, A. E., et al. 2003, ApJ, 592, 728
- Stone, R. C., 1997, AJ, 114, 2811
- Veron-Cetty M.P., Veron P., 2006, A&A, 455, 773
- Wynne, C. G., 1996, MNRAS, 280, 555